Nucleic Acids Research, 2020 **1**
doi: 10.1093/nar/gkaa599

Targeted DNA oxidation by LSD1–SMAD2/3 primes TGF-β1/ EMT genes for activation or repression

Antonio Pezone[1,*,†], Maria Letizia Taddei[2,†], Alfonso Tramontano[3,†], Jacopo Dolcini[1,4], Francesca Ludovica Boffo[1], Mariarosaria De Rosa[1], Matteo Parri[5], Stefano Stinziani[5], Giuseppina Comito[5], Antonio Porcellini[6], Giovanni Raugei[5], Daniel Gackowski[7], Ewelina Zarakowska[7], Ryszard Olinski[7], Armando Gabrielli[4], Paola Chiarugi[5,8,*] and Enrico Vittorio Avvedimento[1,*]

[1]Dipartimento di Medicina Molecolare e Biotecnologie Mediche, Istituto di Endocrinologia ed Oncologia Sperimentale del CNR , Università Federico II, 80131 Napoli, Italy, [2]Dipartimento di Medicina Sperimentale e Clinica, Università degli Studi di Firenze, viale Morgagni 50, 50134 Firenze, Italy, [3]Department of Precision Medicine, University of Campania "L. Vanvitelli", 80138, Naples, Italy, [4]Dipartimento di Scienze Cliniche e Molecolari, Clinica Medica, Università Politecnica delle Marche, 60100, Ancona, Italy, [5]Dipartimento di Scienze Biomediche, Sperimentali e Cliniche, Università degli Studi di Firenze, viale Morgagni 50, 50134 Firenze, Italy, [6]Dipartimento di Biologia , Università Federico II, 80131 Napoli, Italy, [7]Department of Clinical Biochemistry, Faculty of Pharmacy, Collegium Medicum in Bydgoszcz, Nicolaus Copernicus University in Toruń, 85-095 Bydgoszcz, Poland and [8] Tuscany Tumor Institute and Excellence Centre for Research, Transfer and High Education DenoTHE, 50134, Florence, Italy

Received March 17, 2020; Revised June 24, 2020; Editorial Decision June 25, 2020; Accepted July 03, 2020

ABSTRACT

The epithelial-to-mesenchymal transition (EMT) is a complex transcriptional program induced by transforming growth factor β1 (TGF-β1). Histone lysine-specific demethylase 1 (LSD1) has been recognized as a key mediator of EMT in cancer cells, but the precise mechanism that underlies the activation and repression of EMT genes still remains elusive. Here, we characterized the early events induced by TGF-β1 during EMT initiation and establishment. TGF-β1 triggered, 30–90 min post-treatment, a nuclear oxidative wave throughout the genome, documented by confocal microscopy and mass spectrometry, mediated by LSD1. LSD1 was recruited with phosphorylated SMAD2/3 to the promoters of prototypic genes activated and repressed by TGF-β1. After 90 min, phospho-SMAD2/3 downregulation reduced the complex and LSD1 was then recruited with the newly synthesized SNAI1 and repressors, NCoR1 and HDAC3, to the promoters of TGF-β1-repressed genes such as the Wnt soluble inhibitor factor 1 gene (*WIF1*), a change that induced a late oxidative burst. However, TGF-β1 early (90 min) repression of transcription also required synchronous signaling by reactive oxygen species and the stress-activated kinase c-Jun N-terminal kinase. These data elucidate the early events elicited by TGF-β1 and the priming role of DNA oxidation that marks TGF-β1-induced and -repressed genes involved in the EMT.

INTRODUCTION

The epithelial-to-mesenchymal transition (EMT) is the product of a complex transcriptional program that induces mesenchymal characteristics in polarized epithelial cells. These features include reduced cell–cell contacts, enhanced migratory and invasive capacity, and resistance to apoptosis (1). EMT occurs during tumor progression to generate metastatic cells that are endowed with a more motile and invasive phenotype (2). Several transcription factors are implicated in EMT control; particularly, the repressor SNAI1, a member of the zinc finger transcription factor family, is induced by transforming growth factor β1 (TGF-β1) to initiate the EMT transcription program (3). EMT also critically depends on reactive oxygen species (ROS), which support tumor growth by stimulating multiple pathways (4–6). Additionally, high oxidative stress levels in the tumor microenvironment, due to both hypoxia and stromal inflammatory cell recruitment, can promote myofibrob-

*To whom correspondence should be addressed. Tel: +39 0817463614; Email: antoniopezone@gmail.com; antonio.pezone@unina.it
Correspondence may also be addressed to Paola Chiarugi. Tel: +39 0552751247; Email: paola.chiarugi@unifi.it
Correspondence may also be addressed to Enrico Vittorio Avvedimento. Tel: +39 0817463251; Email: avvedim@unina.it
†The authors wish it to be known that, in their opinion, the first three authors should be regarded as Joint First Authors.

last differentiation into activated cancer-associated fibroblasts (CAFs) (7–9). CAFs, in turn, exploit the oxidative stress to produce cytokines and proteases that can elicit EMT in cancer cells (10). Moreover, CAFs induce EMT in prostate carcinoma cells through a redox-dependent mechanism that involves nuclear factor κB (NF-κB), NADPH oxidase (NOX), cyclooxygenase and hypoxia-inducible factor 1 (HIF-1) to sustain tumor progression and metastatic dissemination (11).

ROS and DNA oxidation are also linked to transcription. Demethylation of histone H3 by histone lysine-specific demethylase (LSD1) is stimulated by estrogen and retinoic acid. ROS produced by LSD1 induce oxidation of deoxy-G (oxo-dG), a process that is instrumental for the assembly of a productive transcriptional initiation complex and the formation of transcriptional loops (12,13). In this scenario, the aim of our work was to explore whether a similar mechanism, dependent on nuclear ROS production, could be the driving force behind the transcriptional program leading to EMT in mammary epithelial cells induced by TGF-β1 during the initiation of EMT.

We report here that TGF-β1 triggers an early (30 min) oxidative wave in the nucleus, mediated by LSD1, recruited and targeted by phosphorylated SMAD2/3 to the promoters of activated and repressed TGF-β1/EMT genes. At 90 min, there was a second oxidative wave, detected by the accumulation of oxo-dG glycosylase, OGG1, only at TGF-β-repressed genes. At these promoters, a repressive complex was formed by LSD1 and HDAC3–NCoR1 with the newly synthesized repressor SNAI1. Early (30–90 min) DNA oxidation mediated by LSD1 was necessary for both activation and repression of transcription by TGF-β1. Transcriptional repression by TGF-β1 required an additional signal generated by the ROS-activated kinase c-Jun N-terminal kinase (JNK).

MATERIALS AND METHODS

Materials

PVDF membrane was obtained from Millipore (Bedford, MA, USA); anti-E-cadherin, anti-N-cadherin, anti-SET7/9, anti-OGG1/2, anti-HDAC3, LSD1 shRNA plasmid and JMJD2a shRNA plasmid were obtained from Santa Cruz Biotechnology (Santa Cruz, CA, USA); anti-FLAG and anti-smooth muscle actin antibody and Phalloidin-TRITC were obtained from Sigma-Aldrich (St Louis, MO, USA); DCFDA and Alexa 488 secondary antibody were obtained from Molecular Probes; anti-H3K4me2, anti-H3K4me3, anti-H3K9me2, anti-H3K9me3, anti-H3, anti-LSD1, anti-JMJD2A, anti-SUV39H1, anti-NCoR1, anti-APE1, anti-β-actin, anti-β-tubulin antibodies, anti-IgG mouse and anti-IgG rabbit were obtained from Abcam (Cambridge, UK); anti-pSMAD2/3 (Ser 423/425) and anti-SMAD2/3 antibodies were obtained from Cell Signaling Technology (Danvers, MA, USA); anti-8-oxo-dG antibodies were obtained from Trevigen Inc. (Gaithersburg, MD, USA); and the OxyDNA assay was obtained from Calbiochem (San Diego, CA, USA).

Cell cultures, transfections and drug pretreatments

MCF10A cells were obtained from the American Type Culture Collection. MCF10A cells were cultured in DMEM/Ham's F12 supplemented with 5% horse serum, 0.5 μg/ml hydrocortisone, 100 ng/ml cholera toxin, 20 ng/ml EGF and 10 μg/ml insulin. Before TGF-β1 stimulation, the cells were starved in serum-free medium containing DMEM/Ham's F12 supplemented with 0.5 μg/ml hydrocortisone, 100 ng/ml cholera toxin, 20 ng/ml EGF and 10 μg/ml insulin for 24 h. TGF-β1 (10 ng/ml) was added to the cultures at different times (30–60–90 min or 12–24 h). Where necessary, MCF10A cells were pretreated with *N*-acetylcysteine (NAC, 5 mM), diphenyleneiodonium (DPI, 10 μM), tranylcypromine (TCP, 0.5–1 mM), JIB04 (23 mM), SP600125 (10 μM), SB431542 (10 μM), apocynin (50 μM) and rotenone (5 μM). Several LSD1 inhibitors, SP2509 and CBB1007 (noncatalytic, reversible inhibitors) and OG-L002 and GSK (catalytic MAO inhibitors) (see selleckchem.com/lsd1.html), were tested on MCF10A cells. All of them but TCP reduced the growth at 24–36 h of MCF10A cells at concentrations used (A. Pezone, unpublished data) (14,15).

LSD1–JMJD2A silencing

MCF10A cells were transfected with LSD1 or JMJD2A shRNA/hairpin vectors using Lipofectamine 3000 (Invitrogen, Waltham, MA, USA) according to manufacturer's instructions or by electroporation. Four single or pooled shRNA/hairpin vectors (Santa Cruz Biotech, LSD1sh sc-60970 and JMJD2A sc-62515) targeting different LSD1 or JMJD2A segments were transfected in MCF10A cells. After 24 h, the cells were exposed to TGF-β1 and the levels of JMJD2A, LSD1, β-actin, GADPH, α-tubulin mRNAs and 18S RNA were measured by qPCR or immunoblot with specific antibodies (except 18S RNA). In some experiments, the wild-type human LSD1 expression vector without the 3′-UTR was included in the transfection to control off-target effects in experiments with single or pooled shRNA/hairpin vectors (Supplementary Figure S2).

Immunoprecipitation and immunoblot analysis

A total of 1×10^6 cells were lysed for 20 min on ice in 500 μl of complete RIPA lysis buffer (50 mM Tris–HCl, pH 7.5, 150 mM NaCl, 1% Nonidet P-40, 2 mM EGTA, 1 mM sodium orthovanadate, 1 mM phenylmethylsulfonyl fluoride, 10 μg/ml aprotinin, 10 μg/ml leupeptin). Lysates were clarified by centrifugation and immunoprecipitated for 4 h at 4°C with 1–2 μg of the specific antibodies. Immune complexes were collected on Protein A/G PLUS agarose, separated by SDS-PAGE and transferred onto nitrocellulose. Immunoblots were incubated in 3% milk, 10 mM Tris–HCl, pH 7.5, 1 mM NaCl and 0.1% Tween 20 for 1 h at room temperature, probed first with specific antibodies and then with secondary antibodies.

Real-time PCR

Total RNA from MCF10A was extracted using TRIzol (Gibco/Invitrogen). mRNA was reverse transcribed for 1

h at 50°C, and the reaction was heat inactivated for 15 min at 70°C. The primers used are shown in Supplementary Table S1. Data were normalized to 18S RNA. Results (mean ± SD) are the mean of three different experiments in triplicate.

Immunocytochemistry

After washing with phosphate-buffered saline (PBS), cells were fixed with 3.7% formaldehyde solution in PBS for 20 min at 4°C. After extensive washing in PBS, cells were permeabilized with 0.1% Triton X-100 in PBS and then stained with anti-E-cadherin antibody overnight and with 50 μg/ml fluorescent phalloidin conjugate, phalloidin-TRITC, in PBS for 1 h at room temperature and then with anti-rabbit Alexa 488 secondary antibodies. After washing with PBS, the cover slides were mounted with glycerol and then observed under a confocal fluorescence microscope (Leica Microsystems).

8-Oxo-G assay

Immunocytochemistry was performed according to the manufacturer's instructions (Trevigen Inc.). The anti-8-oxo-dG antibodies (mouse monoclonal 15A3) were validated by confocal microscopy (16) and chromatin immunoprecipitation (ChIP) (17). The signal was resistant to RNase A and sensitive to DNase I and NAC. Briefly, cells were fixed for 15 min with MeOH at −20°C followed by 15 min at −20°C with acetone. Fixed cells were treated with 0.05 N HCl for 5 min on ice and incubated with 250 μl of 100 μg/ml RNase A in 150 mM NaCl and 15 mM sodium citrate for 1 h at 37°C. After sequentially washing in 1× PBS and 35%, 50% and 75% ethanol (EtOH), DNA was denatured *in situ* with 250 μl of 0.15 N NaOH in 70% EtOH. A 0.2 μg/ml (250 μl) TO-PRO-3 Iodide (Thermo Fisher Scientific) in 1× PBS was used to stain DNA for 10 min. After several washing with 70% EtOH containing 4% v/v formaldehyde, 50% and 35% EtOH, and 1× PBS, the cells were incubated in 250 μl of 5 μg/ml proteinase K in 20 mM Tris and 1 mM EDTA, pH 7.5 (TE), for 10 min at 37°C. Nonspecific binding was prevented by incubation with 5% normal goat serum in 1× PBS for 1 h at room temperature. Then, fixed cells were incubated with 250 μl anti-8-hydroxyguanine antibody at a concentration of 1:250 diluted in 1× PBS containing 1% bovine serum albumin (BSA) and 0.01% Tween 20 at 4°C overnight in a humidified chamber. After several washing with 1× PBS containing 0.05% Tween 20, fixed cells were incubated cells in 250 μl of fluorescent secondary antibody, goat anti-mouse IgG (Alexa Fluor 488), at 5 μg/ml in 1× PBS containing 1% BSA for 1 h in the dark at room temperature. After extensive washing, cells were mounted with glycerol and observed by a laser scanning confocal microscope.

Colocalization of 8-oxo-G signals in confocal microscopy

Colocalization of confocal images was performed with two specific plugins of ImageJ: (i) Colocalisation (http://www.sussex.ac.uk/gdsc/intranet/pdfs/Colocalisation.pdf) and (ii) Coloc_2 (https://imagej.net/Coloc_2). Briefly, two points colocalized if their ratio of intensity was higher than the setting value (50 was used as default setting value). To normalize to the number of the cells in each field, the values were expressed as the percentage of the area of the cell nuclei in each individual photo. The area of non-colocalized green spots was measured as percentage of the area of the nuclei. For each sample, Pearson's correlation and Manders' split coefficient were calculated.

Intracellular ROS determination

Production of intracellular H_2O_2 was assayed as previously described (18). At 3 min before the end of the incubation time, DCFDA was added to a final concentration of 5 μM. Cells were lysed in 1 ml of RIPA buffer and analyzed immediately by fluorescence analysis using a Perkin Elmer Fluorescence Spectrophotometer 650-10S equipped with a xenon power supply (excitation 488 nm, emission 510 nm).

2D ultra-performance liquid chromatography–tandem mass spectrometry

The 2D ultra-performance liquid chromatography–tandem mass spectrometry (UPLC–MS/MS) analysis was performed following our recently developed method (19). Briefly, DNA hydrolysates were spiked with a mixture of internal standards in a volumetric ratio of 4:1, to concentration of 50 fmol/μl of [D3]-5-hydroxymethyl-dC (5-hmdC), [$^{13}C_{10}$, $^{15}N_2$]-5-formyl-2′-deoxycytidine, [$^{13}C_{10}$, $^{15}N_2$]-5-carboxyl-2′-deoxycytidine, [$^{13}C_{10}$, $^{15}N_2$]-5-hydroxymethyl-2′-deoxyuridine (5-hmdU) and [$^{15}N_5$]-8-oxo-dG. Chromatographic separation was performed with a Waters Acquity 2D UPLC system with a photodiode array detector, for the first-dimension chromatography, used for the quantification of unmodified deoxynucleosides and 5-methyl-2′-deoxycytidine, and a Xevo TQ-S tandem quadrupole mass spectrometer for the second-dimension chromatography. An at-column dilution technique was used between first and second dimensions for improving retention at the trap/transfer column. The columns used were a Phenomenex Kinetex C-18 column (150 mm × 2.1 mm, 1.7 μm) at the first dimension, a Waters X-select C18 CSH (30 mm × 2.1 mm, 1.7 μm) at the second dimension and Waters X-select C18 CSH (30 mm × 2.1 mm, 1,7 μm) as the trap/transfer column. The chromatographic system operated in the heart-cutting mode, indicating that selected parts of effluent from the first dimension were directed to the trap/transfer column via six-port valve switching, which served as 'injector' for the second-dimension chromatography system. The flow rate at the first dimension was 0.25 ml/min and the injection volume was 0.5–2 μl. The separation was performed with a gradient elution for 10 min using a mobile phase of 0.1% acetate (A) and acetonitrile (B) (1–5% B for 5 min, column washing with 30% acetonitrile and re-equilibration with 99% A for 3.6 min). The flow rate at the second dimension was 0.35 ml/min. The separation was performed with a gradient elution for 10 min using a mobile phase of 0.01% acetate (A) and methanol (B) (4–50% B for 4 min, isocratic flow of 50% B for 1.5 min and re-equilibration with 96% A up to next injection). All samples were analyzed in three to five technical replicates of which technical mean

was used for further calculation. Mass spectrometric detection was performed using the Waters Xevo TQ-S tandem quadrupole mass spectrometer, equipped with an electrospray ionization source. Collision-induced dissociation was obtained using argon 6.0 at 3×10^{-6} bar pressure as the collision gas. Transition patterns for all the analyzed compounds as well as specific detector settings were determined using the MassLynx 4.1 IntelliStart feature.

Chromatin immunoprecipitation

MCF10A cells were grown to 95% confluence in DMEM/Ham's F12. Following the addition of 10 ng/ml TGF-β1 for 30, 60 and 90 min, cells were washed twice with PBS and cross-linked with 1% formaldehyde at room temperature for 10 min. Cells then were washed with ice-cold PBS containing protease inhibitors (1 mM phenylmethylsulfonyl fluoride, 1 μg/ml aprotinin and 1 μg/ml pepstatin A). Cells were then resuspended in 0.2 ml of lysis buffer (1% SDS, 10 mM EDTA, 50 mM Tris–HCl, pH 8.1, 1 mM phenylmethylsulfonyl fluoride, 1 μg/ml aprotinin and 1 μg/ml pepstatin A), sonicated for 17 cycles (12 s followed by 28 s of stop) and centrifuged for 10 min at 10 000 × *g* at 4°C. Supernatants were collected and diluted in buffer containing 1% Triton X-100, 2 mM EDTA, 150 mM NaCl and 20 mM Tris–HCl, pH 8.1. Immunoprecipitation was performed overnight at 4°C with 2 μg of specific antibodies with 14 μl Protein G Dynabeads (Invitrogen, Waltham, MA, USA). After immunoprecipitation, precipitates were washed sequentially for 10 min each in high-salt solution (0.1% SDS, 1% Triton X-100, 2 mM EDTA, 20 mM Tris–HCl, pH 8.1, 150 mM NaCl), low-salt solution (0.1% SDS, 1% Triton X-100, 2 mM EDTA, 20 mM Tris–HCl, pH 8.1, 500 mM NaCl) and LiCl solution (0.25 M LiCl, 1% NP-40, 1% deoxycholate, 1 mM EDTA, 10 mM Tris–HCl, pH 8.1). Precipitates were then washed three times with TE buffer and extracted two times with 1% SDS and 0.1 M $NaHCO_3$. Eluates were pooled and heated at 65°C overnight to reverse the formaldehyde cross-linking. DNA fragments were purified with a QIAquick Spin Kit (Qiagen, Valencia, CA, USA). The primers used are shown in Supplementary Table S1.

Statistical analysis

The data we present derive from at least three biological and three technical replicates. Multivariate analysis of variance (MANOVA) or repeated measures analysis of variance (ANOVA) was used to determine differences in multiple dependent variables over time or between treatments. Each figure is associated with specific statistical figures indicated as Figure *x*-Stat.*y*. Statistical analysis of the data was performed by Student's *t*-test. *P*-values of ≤0.05 were considered statistically significant.

RESULTS

TGF-β1-induced ROS were generated by multiple sources and were all essential for the EMT program

TGF-β1 evokes a time-dependent increase of ROS measured as DCF fluorescence that peaks at 30–45 min after treatment and thereafter declines, although remaining significantly elevated above control even at 120 min post-treatment (Figure 1A and Supplementary Figure 1-Stat.1). As expected, ROS accumulation was sensitive to antioxidant treatments, such as NAC and pegylated catalase (Figure 1B and Supplementary Figure 1-Stat.1). TGF-β1-induced ROS were essential to initiate EMT, as revealed by changes in the levels of N-cadherin, α-SMA and E-cadherin in cells exposed to TGF-β1 and/or NAC (Figure 1C). Confocal microscopic analysis of E-cadherin distribution showed that ROS scavenging by NAC inhibited TGF-β1-induced EMT. Indeed, TGF-β1-treated cells were more dispersed, exhibited an elongated spindle-shaped morphology and displayed well-organized actin stress fibers and reduced E-cadherin levels (Figure 1D and E). NAC treatment inhibited the appearance of these features, data that confirm, in MCF10 cells, EMT induction by TGF-β1 was strictly redox dependent (Figure 1E) (20,21). ROS induced by TGF-β1 are essentially produced by NADPH oxidase(s), specifically NOX4 (22,23). NOX4 is the major NADPH oxidase in MCF10 cells and is induced by TGF-β1 (24–26). A fraction of NOX4 is localized in the mitochondria (27) and is inhibited as the other NOX enzymes by DPI (28).

Loss of cell junctions, due to the switching of cadherin and gene expression reprogramming during EMT establishment, is under tight transcriptional control, which can be regulated by ROS induced by TGF-β1. In this context, the induction of the repressor *SNAI1* by TGF-β1 is an essential and early step to initiate the EMT program (29). To document the link between ROS and early transcriptional changes induced by TGF-β1, we measured the RNA levels of two sets of prototypic genes that are activated or repressed by TGF- β1 in the presence or absence of NAC and DPI (28). These genes were selected from Affymetrix and Illumina microarray platforms on the basis of their strong correlation with other probes involved in EMT in breast and lung cancer cells (30).

Very early upon TGF-β1 exposure (30–90 min), NAC, but not DPI, inhibited *SNAI1* gene expression, data that suggest the ROS required for *SNAI1* induction were not generated by NADPH oxidase (Figure 1F and Supplementary Figure 1-Stat.2–4). The expression of other TGF-β1-induced genes, such as *CDH2* (N-cadherin), *VIM* (vimentin) and *PAI* (serpin1), at 90 min was also resistant to DPI and inhibited by NAC (Figure 1F and Supplementary Figure 1-Stat.2–4). Conversely, the expression of *WIF1*, *MYC* (c-Myc oncogene), *CDH1* (E-cadherin) and *DSP* (desmoplakin 1) genes was repressed by TGF-β1 and reactivated by both NAC and DPI (Figure 1G and Supplementary Figure 1-Stat.5–7). Although DPI is not a specific NOX inhibitor, the different sensitivity of TGF-β-induced and -repressed genes to DPI (not NAC) suggests that ROS induced by TGF-β1 derive from different sources. To link early and late events induced by TGF-β1, we measured the induction of SNAI1 and NOX4 in cells exposed for 24 h to TGF-β1 in the presence or absence of DPI. Supplementary Figure S1B shows that at 24 h the induction of *SNAI* and *NOX4* by TGF-β1 was inhibited by DPI, suggesting that at 24 h both induced and repressed genes were dependent on the same source of ROS induced by TGF-β1, which most likely is NADPH oxidase as found in several cell types (23–25).

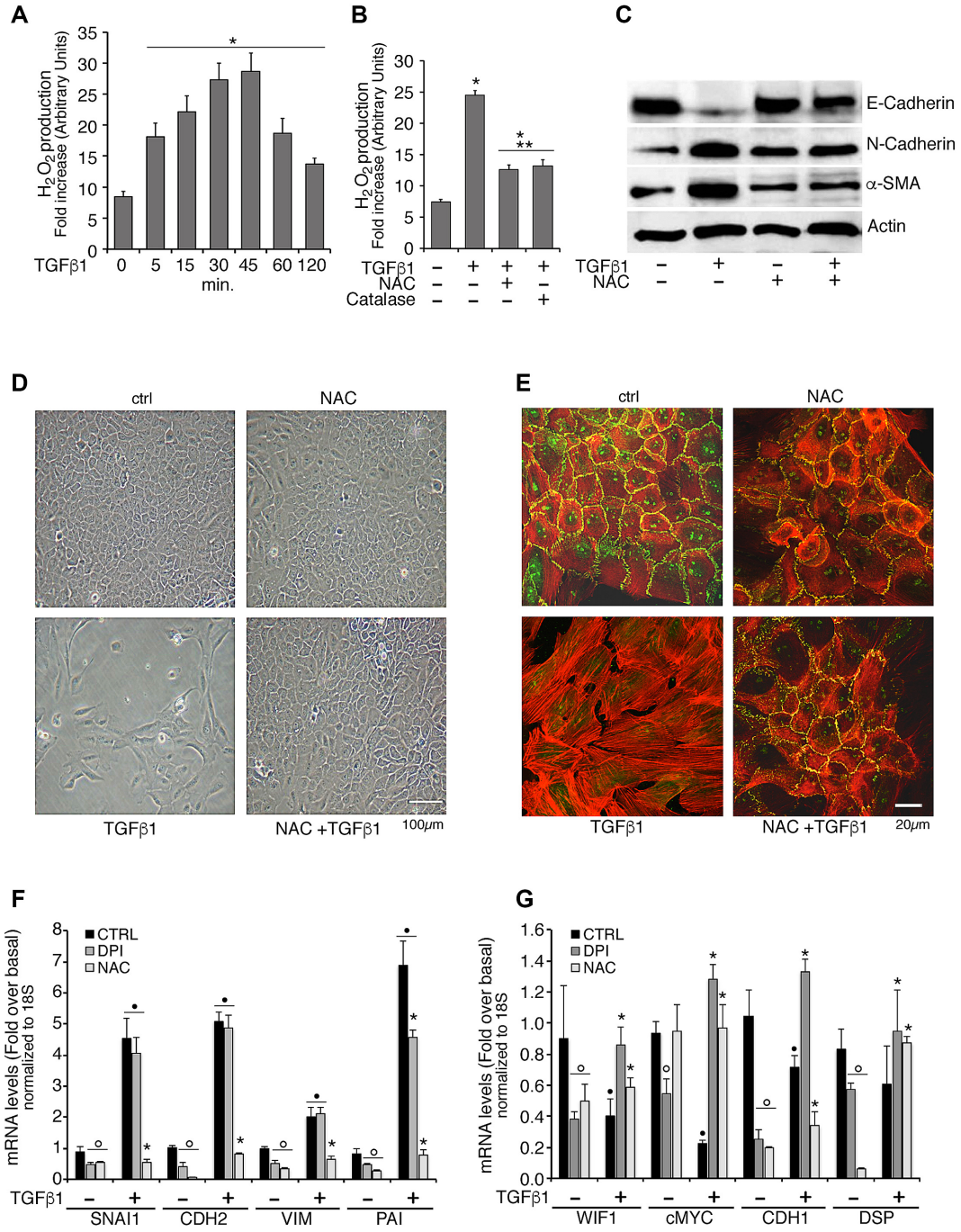

Figure 1. TGF-β1-induced ROS are essential for EMT establishment. (A, B) ROS induced by TGF-β1. (A) Cells were serum starved for 24 h before stimulation with 10 ng/ml TGF-β1 for the indicated times. H_2O_2 production was evaluated as described in the 'Materials and Methods' section. (B) Cells were pretreated with 5 mM NAC or 1 μg/ml catalase for 15 min before stimulation with 10 ng/ml TGF-β1 for 30 min. The data presented are the mean of at least three experiments in duplicate ($n = 6$). Comparison between three or more samples was performed with one-way ANOVA test; comparison between each pairs was performed with Student's *t*-test: $^{*}P < 0.01$ versus untreated control; $^{**}P < 0.01$ versus TGF-β1 alone (see Supplementary Figure 1-Stat.1). (C) E–N cadherin switch and α-SMA levels induced by TGF-β1. Cells were pretreated with 5 mM NAC for 15 min and then stimulated with 10 ng/ml TGF-β1. After 72 h, the cells were lysed and subjected to immunoblot analysis for E-cadherin, N-cadherin, α-SMA and β-actin. (D) Photographs of cells exposed to 10 ng/ml TGF-β1 for 72 h were taken with a phase/contrast microscope. (E) Representative images of cells exposed to 10 ng/ml TGF-β1 for 72 h, fixed and examined by immunofluorescence microscopy of phalloidin in red and E-cadherin in green in the presence of NAC. (F, G) MCF10A cells were pretreated with 5 mM NAC or 5 μM DPI for 15 min before stimulation with 10 ng/ml TGF-β1 for 90 min. Total RNA was extracted and analyzed by qRT-PCR with primers corresponding to SNAI1, CDH2, VIM and PAI mRNA (F) and WIF1, cMYC, CDH1 and DSP genes (Supplementary Table S1) (G). The data shown are the mean of at least three experiments performed three times ($n \geq 9$). A separate MANOVA was used to examine the association between the mRNA levels after TGF-β1 and NAC/DPI treatment; the interaction was significant (see Supplementary Figure 1-Stat.2 for panel F and Supplementary Figure 1-Stat.5 for panel G). Univariate testing found the effect to be significant for both NAC and DPI (see Supplementary Figure 1-Stat.3 for panel F and Supplementary Figure 1-Stat.6 for panel G). $^{*}P < 0.01$ versus CTRL + TGF-β1; $^{\circ}P < 0.01$ versus basal CTRL (without TGF-β1). Pairwise comparison to evaluate the response to TGF-β1 was performed with Student's *t*-test (see Supplementary Figure 1-Stat.4 for panel F and Supplementary Figure 1-Stat.7 for panel G). $^{\bullet}P < 0.01$ versus each basal (without TGF-β1).

Nuclear G oxidation by LSD1 promoted TGF-β1 activation and repression of transcription

To identify the early (30–90 min) ROS sources induced by TGF-β1 that prime the cells to initiate EMT, we focused our attention on the nucleus. Rather than measuring nuclear ROS, which are extremely unstable and diffuse across membranes, we determined the accumulation of the major DNA oxidation product, 8-oxo-dG, by confocal microscopy using specific antibodies against 8-oxo-dG. Figure 2A shows significant accumulation of nuclear 8-oxo-dG after 30-min TGF-β1 treatment, in strict concomitance with the increased ROS levels (Figure 1A) and EMT engagement (Figure 1C). NAC inhibited the oxo-dG levels induced by TGF-β. DPI treatment reduced TGF-β1-induced nuclear 8-oxo-dG and increased the 8-oxo-dG signal, mainly in the perinuclear area (Figure 2A, and Supplementary Figures S1B and S1-Stat.2–3).

8-Oxo-dG has been implicated in transcriptional regulation by a variety of signals, including nuclear hormones such as estrogens (12), retinoic acid (13) and c-Myc (31) or hypoxia (32). Histone demethylation is a redox reaction, and under myriad circumstances it induces deoxy-G oxidation (12,13). The enzymes involved in histone demethylation are mono- or dioxygenases; LSD1 or KDM1 is a monooxygenase that generates hydrogen peroxide during the demethylation reaction (33). Since LSD1 has been associated with EMT engagement and SNAI1-mediated repression of epithelial markers (34), we investigated whether the nuclear oxidation wave induced by TGF-β1 was generated by LSD1. To this end, we silenced LSD1 in MCF10A cells by shRNA (Supplementary Figure S1D) interference and measured 8-oxo-dG upon TGF-β1 stimulation. LSD1 silencing was as effective as NAC (compare Figure 2A and B) at inhibiting TGF-β1-induced deoxy-G oxidation (Figure 2B, and Supplementary Figures S1C and D and S1-Stat.4–5). Additionally, treatment of the cells with a monoamine oxidase inhibitor, namely TCP (15,35), abolished the nuclear 8-oxo-dG signal (Figure 2A and Supplementary Figure S1B). These data showed that LSD1 is the source of nuclear ROS and the cause of G oxidation. As a logical extension of the previous experiment, we analyzed EMT engagement in MCF10A cells upon LSD1 depletion. Confocal analysis of cortical E-cadherin and actin stress fibers confirmed that *LSD1* silencing inhibited EMT induced by TGF-β1 (Figure 2C).

The data reported above show that the nuclear TGF-β1-induced ROS were produced by LSD1 (Figure 2B) and that LSD1 depletion inhibited the EMT/TGF-β1 response (Figure 2C). To document the impact of LSD1 on the expression of the genes involved in EMT, we measured *SNAI1* and other TGF-β1-induced or -repressed mRNA levels in LSD1-depleted cells. LSD1 knockdown abolished *SNAI1* induction as well as the induction of *CDH2*, *VIM* and *PAI* by TGF-β1 (Figure 2D and Supplementary Figure 2-Stat.1–2). Moreover, LSD1 silencing reversed TGF-β1 repression of genes such as *WIF1*, *cMYC*, *CDH1* and *DSP* (Figure 2E and Supplementary Figure 2-Stat.3–4). Furthermore, treatment of the cells with TCP, the monoamine oxidase inhibitor (15,35), inhibited the TGF-β1-mediated induction of *SNAI1*, *CDH2*, *VIM* and *PAI* and prevented the TGF-β1-mediated repression of *WIF1*, *MYC*, *CDH1* and *DSP*, replicating LSD1 depletion effects (Figure 2F, Supplementary Figure 2-Stat.5–6, Figure 2G and Supplementary Figure 2-Stat.7–8). The effects of LSD1 shRNAs on *SNAI1* and *WIF1* induction or inhibition of transcription were prevented by expressing exogenous LSD1 (Supplementary Figure S2).

TGF-β1 induced a genome-wide temporal oxidation wave that modified the DNA

Confocal microscopy revealed that TGF-β1 treatment induced 8-oxo-dG nuclear signal; it was eliminated by LSD1 depletion (Figure 2B). To confirm this finding with a different technique, we subjected the DNA of TGF-β1-exposed cells to MS analysis to identify and quantify the modified DNA bases (see the 'Materials and Methods' section). Figure 3A shows that 8-oxo-dG levels were induced by TGF-β1 after 60–90 min (Figure 3A and Supplementary Figure 3-Stat.1A). Induction of 8-oxo-dG by TGF-β1 was prevented by DPI or LSD1 depletion (Figure 3A and Supplementary Figure 3-Stat.3A and 4A). Apocynin, a nonspecific antioxidant, that inhibits peroxides (36) did not modify the 8-oxo-dG levels induced by TGF-β1 (Figure 3A, right panel, and Supplementary Figure 3-Stat.3).

Analysis of the other modified DNA bases revealed that the TGF-β1 effects on DNA also involve deoxy-C metabolites: 5-hmdC and 5-methyl-dC (Figure 3B and C, and Supplementary Figure 3-Stat.1-2B and C). Furthermore, 5-hmdU or deoxy-U levels were reduced by DPI, data that suggest oxidation by NOX enzymes favors C and T deamination (Figure 3D and E, and Supplementary Figure 3-Stat.1–2D and E and 3-Stat.3).

To our knowledge, these data provide the first demonstration that TGF-β1 induces a genome-wide oxidation wave that modifies DNA to initiate the EMT transcriptional program.

Common and differential chromatin changes induced by TGF-β1 at repressed and activated promoters

The above data demonstrate that LSD1 is required for DNA oxidation and for both the activation and repression of TGF-β1-induced transcription, but they do not clarify the mechanism. TGF-β1-activated receptors I and II induce a series of events that culminate in the phosphorylation and nuclear accumulation of the phosphorylated SMAD2/3 complex (37). We analyzed by ChIP the earliest chromatin changes (30–60 min) at the promoter sites of the two prototypic genes induced (*SNAI1*) or repressed (*WIF1*) by TGF-β1. The analyzed genomic regions contain sequences recognized by the complex SMAD2/3 (37,38) (A. Pezone, unpublished data). Upon TGF-β1 challenge, phosphorylated SMAD2/3 (pSMAD2/3) complex was recruited to the *SNAI1* and *WIF1* promoters and steadily accumulated at 30 min and disappeared by 90 min (Figure 4A and B). LSD1 was also recruited after 30 min at both promoters, but at 90 min, compared to 0- or 60-min treatment, LSD1 accumulated at *WIF1* promoter (Figure 4A and B, and Supplementary Figure 4-Stat.1). The recruitment at 30 min of

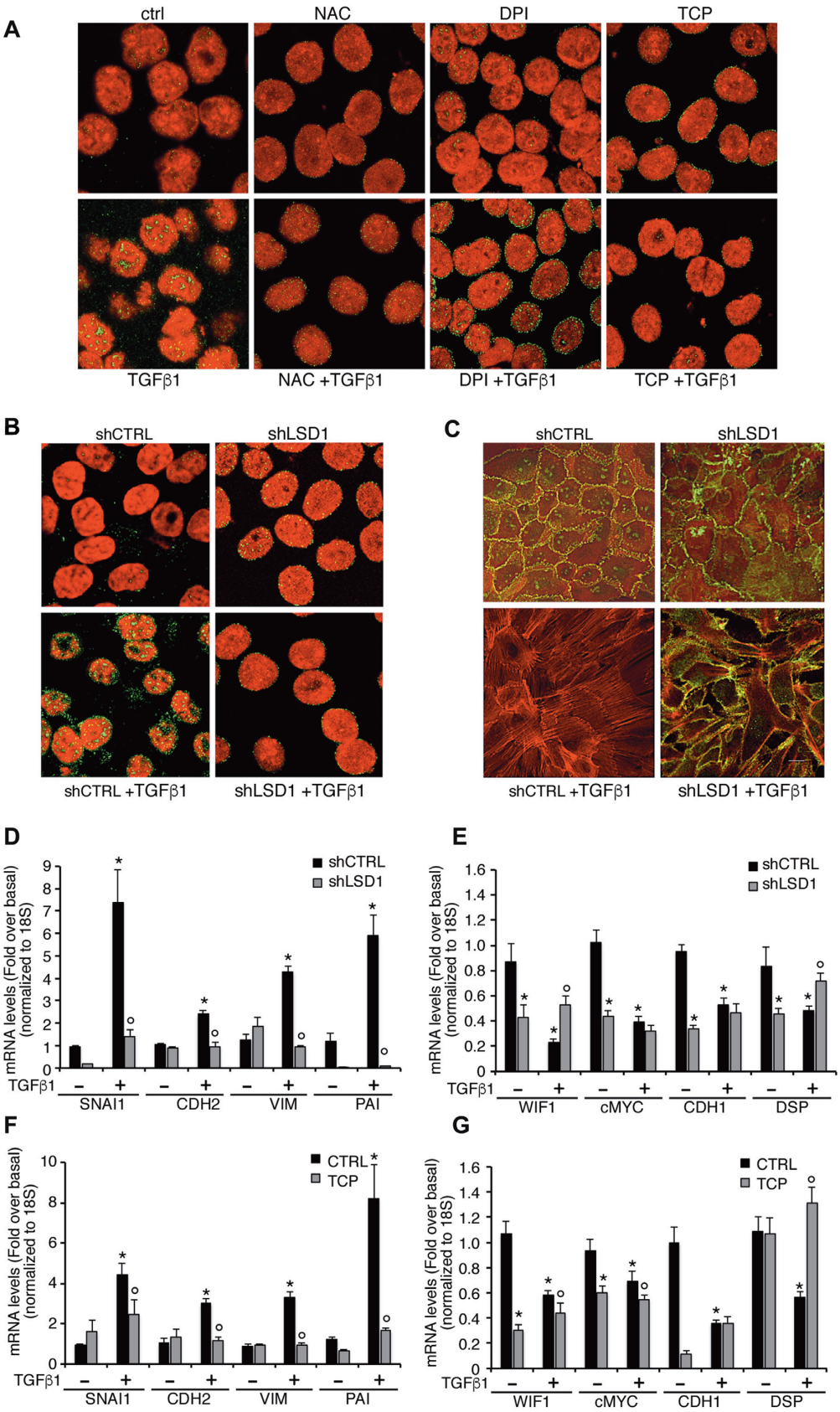

Figure 2. Nuclear G oxidation induced by TGF-β1 through the histone demethylase, LSD1. (A) Immunofluorescence detection of 8-oxo-dG by fluorescein-tagged anti-8-oxo-dG antibody in cells pretreated with 5 mM NAC or 5 μM DPI for 1 h before stimulation with 10 ng/ml TGF-β1 for 30 min. Nuclei

LSD1 and pSMAD2/3 suggests that these proteins form a transient complex at both promoters. The association between LSD1 and pSMAD2/3 was shown by immunoprecipitation with antibodies to LSD1 and immunoblot with anti-pSMAD2/3 (Figure 4D) or immunoprecipitation with antibodies to an exogenous FLAG–LSD1 and western blot with anti-pSMAD2/3 antibodies in extracts derived from transfected cells (Figure 4E). The association was also shown by ChIP and re-ChIP experiments of *SNAI1* and *WIF1* promoters with antibodies against LSD1 on pSMAD2/3 (Figure 4G and H, and Supplementary Figure 4-Stat.2). Both assays (immunoprecipitation and ChIP) revealed that non-phosphorylated SMAD2/3 did not bind LSD1. However, the absence of signal with the antibody to total SMAD2/3 suggests that only a fraction of SMAD2/3 binds LSD1 (Figure 4F). The complex that contained pSMAD2/3 was transient (30 min) and rapidly disappeared at the *SNAI1* promoter between 60 and 90 min after TGF-β1 treatment (Figure 4A). LSD1 reappeared at the *WIF*1 promoter 90 min after TGF-β1 treatment, without pSMAD2/3 (Figure 4B and Supplementary Figure 4-Stat.1C and D). The notion that pSMAD2/3 is recruited to promoters repressed by TGF-β1 is not novel, although it has not been connected to a specific mechanism (36). Phosphorylated SMAD2/3 work as pioneer factors that transiently bind DNA sites present in TGF-β1-induced or -repressed promoters in different cell types (38,39). Depending on the concomitant presence of other signals, such as ROS and stress-kinase-induced repressors (40,41), some genes are repressed while others are activated. For example, the repressor *SNAI1* was induced at 30 min after TGF-β1 challenge and recruited at 90 min to the *WIF1* promoter, where it formed a complex with LSD1 and silenced the expression of the gene (Supplementary Figures S3 and S3-Stat.1A–C). With the same timing, the co-repressors NCoR1 and HDAC3 accumulated at the *WIF* promoter (Supplementary Figures S4A and B, and S4-Stat.1).

Collectively, these data demonstrate that the pSMAD2/3–LSD1 complex very early upon TGF-β1 challenge targeted the chromatin of TGF-β1-activated and -repressed promoters (Figure 4A and B). Ninety minutes after TGF-β1 challenge, SNAI1 and LSD1 accumulated preferentially at the repressed promoters (Figure 4A and B). Since nuclear G oxidation was the earliest modification we observed upon TGF-β1 challenge, we measured recruitment of OGG1 and the apurinic/apyrimidinic endonuclease 1 (APE1) to the *SNAI1* and *WIF1* promoters. OGG1 recognizes 8-oxo-dG and APE1 targets, excises and repairs the abasic site generated by OGG1 (42). Since LSD1 demethylates H3K4 and K9m2, we also determined at the same sites the H3K4-K9 methylation status and the recruitment of H3K9 and H3K4 methyltransferases, SUV39 and SET7/9 (43,44).

In summary, OGG1 accumulated at 30 min at the *SNAI1* promoter (Figure 5A and Supplementary Figure 5-Stat.1A–C) and at 30 and 90 min at the *WIF1* promoter (Figure 5B and Supplementary Figures 5-Stat.1D–F and S3B), a pattern that mirrored the timing of LSD1 recruitment at the same sites (Figure 4A and B). The presence of APE1 at both promoters 90 min after TGF-β1 treatment suggests a prolonged repair step, such as long-patch base excision repair, following dG oxidation (45,46) at both promoters. At *WIF1* promoter, the second oxidation peak is marked by OGG1 and overlaps with the rise of 8-oxo-dG levels at 90 min detected by MS (Figure 3A). With the same timing, NCoR1 and HDAC3 accumulate at the *WIF1* promoter (Supplementary Figure S4B). Since the TGF-β1-induced dG oxidation is dependent on LSD1 (Figures 2 and 3) and LSD1 demethylates H3K9 and H3K4m2 (12,13), we have asked whether LSD1 contributes to the H3K9 and H3K4 methylation status of *SNAI1* and *WIF1* chromatin during the early response to TGF-β1. Histone H3 methylation changes induced by TGF-β1 at the *SNAI1* and *WIF1* promoters are produced by the recruitment of demethylases and methyltransferases (43,44). Following TGF-β1 stimulation, both K9 and K4 methyltransferases, SUV39 and SET7/9, respectively, were recruited to the *SNAI1* and *WIF1* promoters with similar kinetics (Supplementary Fig-

←

were stained with TO-PRO-3 Iodide in red while 8-oxo-dG foci were stained in green, as described in the 'Materials and Methods' section. Fluorescence quantization and statistical analysis are shown in Supplementary Figures S1C and S1-Stat3–6. (B) Immunofluorescence detection of 8-oxo-dG by fluorescein-tagged anti-8-oxo-dG antibody in cells transfected with scrambled short hairpin (shCTRL) and shLSD1 RNAs for 24 h before stimulation with 10 ng/ml TGF-β1 for 30 min. Nuclei were stained with TO-PRO-3 Iodide in red while 8-oxo-dG foci were stained in green. Colocalization was measured using ImageJ (Coloc_2 plugin) as described in the 'Materials and Methods' section. Fluorescence quantization and statistical analysis are shown in Supplementary Figures S1D and S1-Stat3–6. (C) Immunofluorescence microscopy of phalloidin in red and E-cadherin in green in control or LSD1-depleted cells exposed to 10 ng/ml TGF-β1 for 72 h. (D–G) mRNA levels of genes regulated by TGF-β1 in cells treated with shLSD1 or with TCP. Results are the mean of at least three experiments performed three times ($n = 9$). MANOVA was used to examine the association between the mRNA levels after TGF-β1 and LSD1 depletion; the interaction was significant (see Supplementary Figure 2-Stat.2 for panel D and Supplementary Figure 2-Stat.4 for panel E). Differences between the means of three or more groups were determined by MANOVA. Differences between three or more samples were determined by one-way ANOVA test. Pairwise comparison was performed with Student's *t*-test (see Supplementary Figures -Stat). (D) mRNA levels of SNAI1, CDH2, VIM and PAI genes in cells induced for 90 min with TGF-β1 determined by qPCR. Total RNA was isolated, reverse transcribed and amplified by qPCR with specific primers (Supplementary Table S1). The values were normalized to 18S RNA. RNA was isolated as described in the 'Materials and Methods' section. $^{*}P < 0.01$ versus basal (without TGF-β1); $^{\circ}P < 0.01$ versus TGF-β1 alone. The actual *P*-values are shown in Supplementary Figure 2-Stat.1. (E) mRNA levels of WIF1, cMYC, CDH1 and DSP1 genes in cells induced for 90 min with TGF-β1. The values were normalized to 18S RNA. $^{*}P < 0.01$ versus basal (without TGF-β1); $^{\circ}P < 0.01$ versus TGF-β1 alone. The actual *P*-values are shown in Supplementary Figure 2-Stat.3. (F) mRNA levels of SNAI1, CDH2, VIM and PAI genes in cells induced for 90 min with TGF-β1 by qPCR. MCF10A cells were pretreated with TCP (1 μg/ml) for 60 min and stimulated with 10 ng/ml TGF-β1 for 90 min. The values were normalized to 18S RNA. $^{*}P < 0.01$ versus basal (without TGF-β1); $^{\circ}P < 0.01$ versus TGF-β1 alone. The actual *P*-values are shown in Supplementary Figure 2-Stat.5. (G) mRNA levels of WIF1, cMYC, CDH1 and DSP1 genes in cells induced for 3 h with TGF-β1 and pretreated with TCP (1 μg/ml) for 60 min. The values were normalized to 18S RNA. $^{*}P < 0.01$ versus basal (without TGF-β1); $^{\circ}P < 0.01$ versus TGF-β1 alone. The actual *P*-values are shown in Supplementary Figure 2-Stat.7. Association between the mRNA levels after TGF-β1 and TCP treatment was significant (for MANOVA, see Supplementary Figure 2-Stat.6 for panel F and Supplementary Figure 2-Stat.8 for panel G).

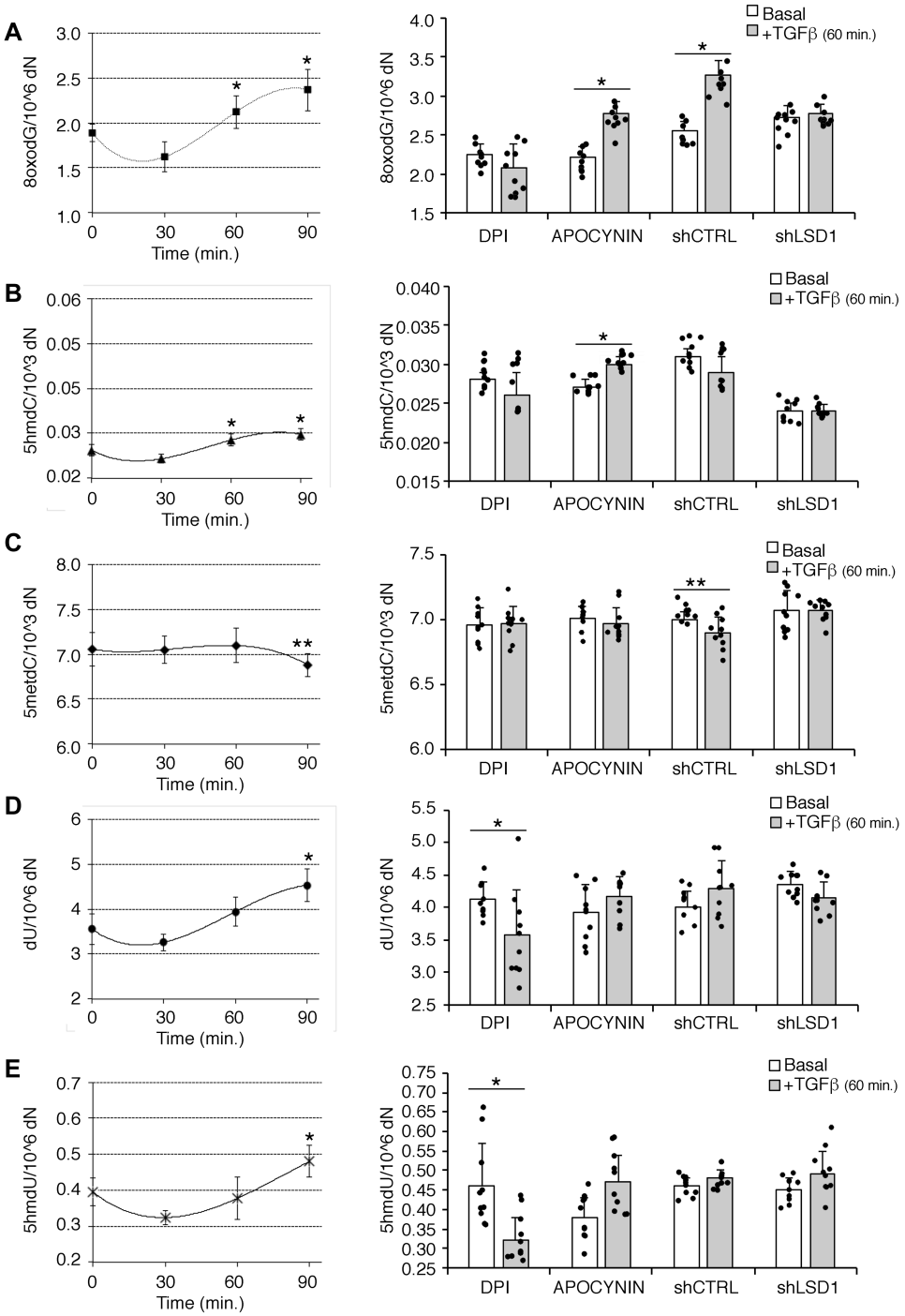

Figure 3. 2D UPLC–MS/MS analysis of DNA derived from cells stimulated with TGF-β1 for various periods of time (left panels) or for 60 min in the presence of DPI, apocynin, shCTRL or shLSD1 (right panels). The technical and statistical details are indicated in the 'Materials and Methods' section and in Supplementary Figure 3-Stat.1–5. Results are the mean of at least three experiments in triplicate ($n \geq 9$). Left panels: Multivariate analysis of repeated measures (RM-MANOVA) was used to determine differences in multiple dependent variables over time. Pairwise comparison was performed with Student's *t*-test. $^*P < 0.01$ versus time zero. The actual *P*-values are shown in Supplementary Figure 3-Stat.1–2. Right panels: The effect of TGF-β1 in the various treatment conditions was evaluated with the Wilcoxon signed-rank test (Supplementary Figure 3-Stat.3). Differences between three or more groups were determined by MANOVA (Supplementary Figure 3-Stat.4–5).

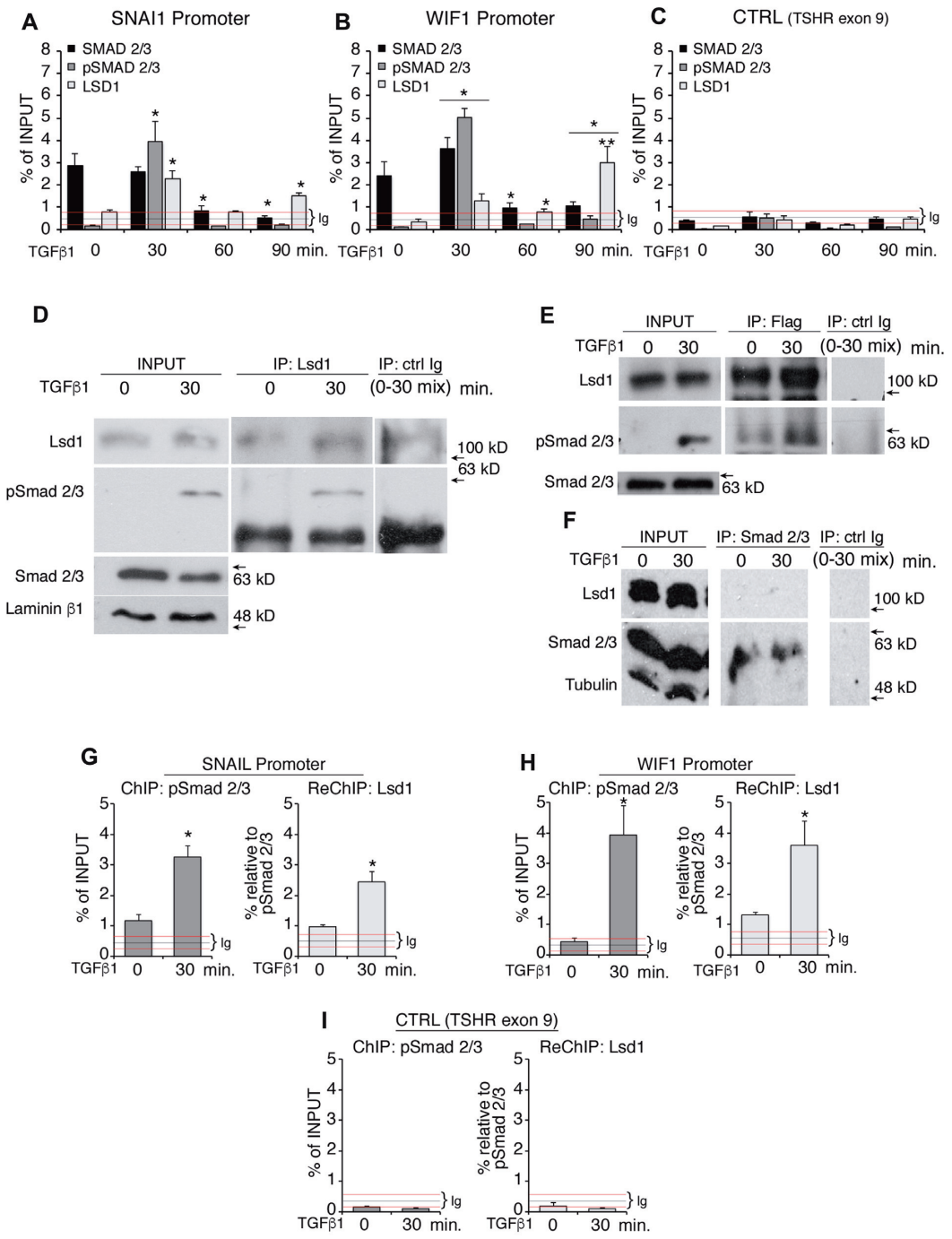

Figure 4. TGF-β1-induced phospho-SMAD2/3 interact with LSD1 and form a transient complex at the WIF1 and SNAI1 promoters. Chromatin from MCF10A cells stimulated with 10 ng/ml TGF-β1 for 30, 60 and 90 min was immunoprecipitated with antibodies to SMAD2/3 or phospho-SMAD2/3, anti-LSD1. DNA was extracted and amplified with primers corresponding to *SNAI1* (A) or *WIF1* (B) promoters or as control the promoter region of human TSH receptor gene, *TSHR* (C). Normal mouse or rabbit pre-immune IgG was used as a negative control (horizontal lines in each graph). The bar graph shows the qPCR signals in immunoprecipitates, normalized to input DNA from each sample. Multivariate analysis of repeated measures (RM-MANOVA) was used to determine differences in multiple dependent variables over time (Supplementary Figure 4-Stat.1A, C and E). Differences between three or more samples were determined by one-way ANOVA test; pairwise comparison was performed with Student's *t*-test (Supplementary Figure 4-Stat.1B, D and F). $^{*}P < 0.01$, in 90-, 60- or 30-min TGF-β1-stimulated cells versus control. $^{**}P < 0.01$, in 90-min compared to 60-min TGF-β1-treated cells. The primers used are shown in Supplementary Table S1. (D) Immunoprecipitation of LSD1 and immunoblot with anti-phospho-SMAD2/3, LSD1, SMAD2/3 and LAMININ β1 antibodies in cells exposed for 30 min to TGF-β1. (E) Immunoprecipitation of exogenous FLAG–LSD1 with anti-FLAG antibodies and immunoblot with anti-phospho-SMAD2/3 and SMAD2/3. (F) Immunoprecipitation of SMAD2/3 and immunoblot with LSD1, SMAD2/3 and tubulin antibodies in cells exposed for 30 min to TGF-β1. ChIP of *SNAI1* (G), *WIF1* (H) and *TSHR* (I) gene promoters with antibodies versus phospho-SMAD2/3. The DNA immunoprecipitated was subjected to re-ChIP with anti-LSD1 antibody. Data are reported as mean ± SD of three experiments in triplicate ($n = 9$). Pairwise comparison was performed with Student's *t*-test. $^{*}P < 0.01$, TGF-β1-stimulated cells versus control (Supplementary Figure 4-Stat.2). The primers are shown in Supplementary Table S1.

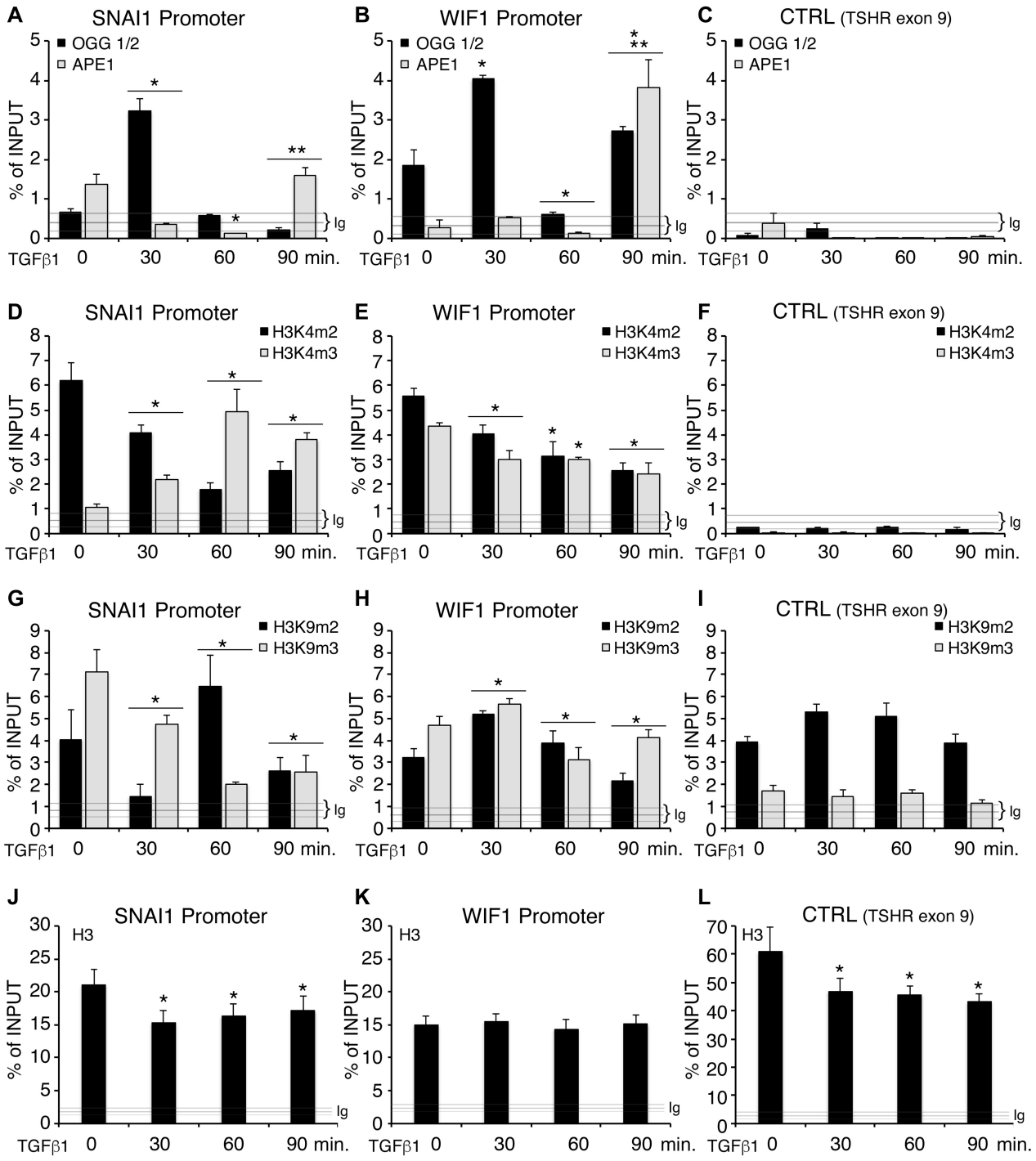

Figure 5. Chromatin changes induced by TGF-β1 at repressed and activated promoters. Chromatin from MCF10A cells stimulated with 10 ng/ml TGF-β1 for 30, 60 and 90 min was immunoprecipitated with antibodies to OGG1 or APE1 (A–C), anti-H3K4me2/3 (D–F), anti-H3K9me2/3 (G–I) or anti-H3 (J–L). DNA was extracted and amplified with primers corresponding to *SNAI1* (left panels) or *WIF1* (middle panels) promoters or as control the promoter region of human TSH receptor gene, *TSHR* (right panels). Normal mouse or rabbit pre-immune IgG was used as a negative control (horizontal lines in each graph). The bar graph shows the qPCR signals in immunoprecipitates, normalized to input DNA from each sample. Data are reported as mean ± SD of three experiments, performed, at least, in triplicate ($n \geq 9$). Multivariate analysis of repeated measures (RM-MANOVA) was used to determine differences in multiple dependent variables over time (Supplementary Figure 5-Stat.1–3A, D and G). Differences between three or more samples were determined by one-way ANOVA test (Supplementary Figure 5-Stat.1–3). Pairwise comparison was performed with Student's *t*-test. *$P < 0.01$, in 90-, 60- or 30-min TGF-β1-stimulated cells versus control. **$P < 0.01$, in 90-min compared to 60-min TGF-β1-treated cells. The primers used are shown in Supplementary Table S1.

ures S4D and E, and S4-Stat.2). In contrast, H3K9me2–3 and H3K4me2–3 levels at the same promoters varied considerably between 30 and 90 min after TGF-β1 treatment (Figure 5D and E). Briefly, the most prominent H3K4 and K9 methylation changes upon TGF-β1 treatment are the following: (i) A time-dependent increase of H3K4me3 at *SNAI1* promoter (Figure 5D and E) due to methylation of H3K4me2 (Supplementary Figures S4D and S4-Stat.2). (ii) A progressive reduction of H3K4me2 and H3K4me3 at *WIF1* promoter, due to H3K4me2 and H3K4me3 demethylation, notwithstanding the rise at 90 min of the methyltransferase SET7/9 (Figure 5E, and Supplementary Figures S4E and S4-Stat.2). These changes are consistent with the induction of *SNAI1* and the inhibition of *WIF1* expression by TGF-β1 treatment. (iii) The monoamine oxidase inhibition activity by TCP increased H3K4me2 levels at the *WIF1* (Supplementary Figures S5B and S5-Stat.1–2) and the levels of H3K9m2 at the *SNAI1* promoters (Supplementary Figures S5D and S5-Stat.3), notwithstanding the recruitment of the methyltransferases SUV39 and SET7/9 (Supplementary Figure S4E). Although TCP inhibits nonspecifically monoxidases, it increases the global levels of H3K4me2, which is the natural LSD1 substrate (Supplementary Figure S5J). The methylation changes induced by TCP are consistent with the inhibition of TGF-β1 induction or repression of SNAI1 and WIF1 transcription as in cells in which LSD1 has been depleted (Figure 2D–G). The methylation changes induced by TCP were associated with a significant depletion of nucleosomes at the *WIF1* promoter, as shown by loss of H3 at 30 and 90 min (Supplementary Figures S5H and S5-Stat.4).

Collectively, the levels of H3K9m2 and H3K4m2, the timing of LSD1 recruitment and the effects of TCP on the H3K4m2 and H3K9m2 levels suggest that LSD1 recruitment and activity mediate the induction of *SNAI1* and the repression of *WIF1* by TGF-β1 (Figure 4A and B).

Also, the H3K9me2 reduction of H3K9me2 levels at the chromatin of the *SNAI1* promoter in the first 30 min without a concomitant increase of H3K9me3 (Figure 5G) suggests that H3K9me2 is the main LSD1 substrate at the *SNAI1* promoter, as previously shown at the chromatin of genes induced by nuclear receptors (12,13). Finally, the steady H3K4me3 increase and the concomitant reduction in H3K4me2 after 60 min of TGF-β1 stimulation at the *SNAI1* promoter can be explained by the recruitment of the methyltransferase SET7/9 following 30 min of TGF-β1 stimulation (Figure 5D and Supplementary Figure S4D). The H3K9me2 chromatin modification induced by LSD1 (Figure 5G) was consistent with the loss of TGF-β1 induction and repression of target genes upon LSD1 depletion or TCP exposure (Figure 2D–G).

Cooperation between two histone demethylases, LSD1 and JMJD2A, mediated TGF-β1-induced EMT

LSD1 demethylates H3K4me2 and H3K9me2 but not trimethyl K4 or K9 (47). To account for the H3K9me3 changes at the *SNAI1* and *WIF1* promoters, we determined the effects of TGF-β1 on a different type of histone demethylase, KDM4A (also called JMJD2A or JHDM3A), a dioxygenase that demethylates H3K9me3 and H3K9me2 in an oxidation reaction that requires Fe^{2+} (48). Notably, KDM4A/JMJD2A is exquisitely sensitive to oxygen levels and displays a graded response to oxygen depletion (49). JMJD2A depletion inhibited the nuclear 8-oxo-dG signal and TGF-β1-induced EMT (Supplementary Figure S6A–D). JMJD2A, upon TGF-β1 stimulation, was recruited to the *SNAI1* promoter and marginally to the *WIF1* promoter 30 min after treatment (Supplementary Figure S6I and J). JMJD2A depletion reduced the expression of *SNAI1*, *CDH2*, *VIM* and *PAI* induced by TGF-β1 (Supplementary Figure S6E and F), but did not change TGF-β1-mediated repression of *WIF1*, *MYC*, *CDH1* and *DSP* (Supplementary Figures S6G and H, and S6-Stat.1–7). The same phenotype was observed by inhibiting JMJD2 activity with JIB04 (50,51) (Supplementary Figures S3 and S6-Stat.1–7). We conclude that JMJD2A cooperates with LSD1 to activate TGF-β1-induced EMT genes and it is not required for TGF-β1 silencing of epithelial genes.

Repression of transcription by TGF-β1 is dependent on both nuclear and cytoplasmic ROS

Collectively, the above data demonstrated that LSD1 is involved in both TGF-β1 induction and repression of transcription depending on the histone methylation code and partnership with other factors, such as pSMAD2/3 or SNAI1 recruited at activated or repressed promoters, respectively. ROS are central to both activation and repression of transcription by TGF-β1 (Figure 1F and G), and their source might be relevant for the efficiency of the final transcriptional response.

Early (30–90 min) TGF-β1-mediated transcription induction or repression can be explained by the activation of two major signaling pathways, both of which require LSD1. The first, which leads to transcription activation, includes nuclear ROS, pSMAD2/3, LSD1 and JMJD2A/KDM4A. The second, which represses transcription, is established by the LSD1–SNAI1 complex, and, eventually, maintained by the co-repressors NCoR1–HDAC3 (Figures 1F and G, and 2A, F and G).

To get insight into the other signaling element(s) that cooperate with LSD1 to mediate TGF-β1 transcription repression, we exposed TGF-β1-treated cells to several chemical inhibitors to identify the primary source of the ROS: (i) rotenone (52), an inhibitor of mitochondrial complex I, which has been linked to TGF-β1-induced ROS; (ii) apocynin, which is a generic antioxidant, which does not modify nuclear oxo-dG accumulation by TGF-β, but inhibits peroxides (36,53); and (iii) SP600125, a specific inhibitor of JNK (54), the ROS-activated kinase that mediates *WIF1* silencing by ROS and ATM (41,55).

Although the ROS inhibitors we have used were not as specific as the silencing probes, we can extract the following information: (i) Apocynin prevented repression of transcription by TGF-β1 (Supplementary Figure S7D) but did not reduce oxo-dG detected by MS (Figure 3A). (ii) DPI prevented repression of transcription by TGF-β1 (Figure 1G) and reduced nuclear oxo-dG detected by MS (Figure 3A). (iii) Both drugs did not influence the induction of transcription by TGF- β1 at early times, while an ROS scavenger like NAC prevented both induction and repression of tran-

scription by TGF-β1 (Figure 1F and Supplementary Figure S6C). At 24 h, DPI inhibited *NOX4* and *SNAI* induction by TGF-β1 (Supplementary Figure S1A and B) (26,28,29). (iv) SP600125, the JNK inhibitor, did not influence TGF-β1-induced gene expression (Supplementary Figure S7A), but prevented TGF-β1 silencing of *WIF1*, *MYC*, *CDH1* and *DSP* genes (Supplementary Figures S7B and S7-Stat.1–5), data that replicate the effects of DPI (Figure 1F-G). (v) Unexpectedly, inhibition of mitochondrial complex I by rotenone did not affect early TGF-β1 repression of EMT genes, data that suggest mitochondrial ROS do not mediate TGF-β1 early inhibition of transcription, notwithstanding the presence of SNAI1 repressor (Supplementary Figure S7C and D). These results imply that at 2 and 24 h there are two pharmacologically different sources of ROS induced by TGF-β1. At 24 h, the major player is NOX4 and this has been demonstrated in many laboratories and we now know that NOX4 is induced at 24 h, and its expression is inhibited by DPI (Supplementary Figure S1A) (25,26). At early times, LSD1 is the main source of nuclear ROS and is essential for both induction and repression of transcription by TGF-β1. However, the data shown in Supplementary Figure S7 suggest that another early source of ROS (JNK) is necessary for the early inhibition of transcription by TGF-β1. Here, we provide an experimental tool to separate the induction and repression of transcription by TGF-β1 at early (hours) and late (days) times. Notably, SNAI1, which is considered essential for TGF-β1/LSD1 repression of epithelial genes (31) in the presence of DPI, did not repress early transcription (Figure 1F and G, and Supplementary Figure S7C and D). We believe that this information is relevant because SNAI1 is considered the master repressor of transcription induced by TGF-β1 (31).

DISCUSSION

The role of ROS in the regulation of EMT in several cell types, including tumor models, is the subject of active investigation (5,6). Oxidative stress following the exposure of cells to microenvironmental insults, such as hypoxia or contact with stromal or inflammatory cells (i.e. CAFs or macrophages), has been causally associated with EMT activation. In redox-dependent EMT, there are at least two molecular axes driven by pro-inflammatory/pro-oxidant sensors: one involves HIF-1 and NF-κB and the other involves the Rac-1 small GTPase, NOX and Src kinase (5,6,8). With our data, we identified another element that plays a relevant role in the EMT transcriptional program: ROS induced by TGF-β1 in the nuclear compartment by the histone demethylase LSD1 (Figure 2B) were essential for the induction, repression of transcription and the initiation of the TGF-β1-mediated EMT program (Figures 1 and 2). LSD1 was targeted to promoter sites activated or repressed by TGF-β1 by phospho-SMAD2/3 (Figure 4A and B).

Phosphorylated SMAD2/3 and LSD1 targeted TGF-β1-induced and -repressed genes

Induction of phospho-SMAD2/3 by TGF-β1 is a central event (29,37) that initiates the EMT transcriptional program. Although SMAD2 does not directly bind to DNA, the SMAD2/3 complex recognizes specific, essential sequence motifs present at the transcription start site (TSS) and enhancers of many TGF-β1-induced or -repressed genes (29,37,38). These SMAD2/3 signatures were also present in the TGF-β1-induced or -repressed genes analyzed here. Phosphorylated SMAD2/3 work as a pioneer factors that mark several genomic sites of TGF-β1-induced or -repressed promoters in different cell types (38–40). Depending on the cell context and the presence of other factors, some genes will be induced and others will be inhibited. Our data suggest that the cellular context is represented by different ROS sources.

TGF-β1 genomic oxidative signature initiated the EMT program

TGF-β induces nuclear migration of SMAD proteins, which are phosphorylated by several kinases, including stress kinases, JNK and p38 (41). PhosphoSMAD2/3 complex binds and targets LSD1 to the promoters of genes such as *SNAI1* and *WIF1*, which are induced or repressed, respectively, by TGF-β1 (Figure 4A and B). LSD1 induced a peak of 8-oxo-dG, detectable by recruitment of OGG1 and APE1 at *SNAI1* and *WIF1* promoters (Figure 5A and B). Local dG oxidation at these two promoters reflected a massive oxidation wave across the entire genome induced by TGF-β1, detectable by MS and dependent on LSD1 (Figure 3). G and C are oxidized *in vivo* by two mechanisms. In the first, G is oxidized by a Fenton reaction catalyzed by LSD1, which generates hydrogen peroxide (33), and partly by KDM4A/JMJD2A (dependent on Fe^{2+}) (48). In the second, C is oxidized by ten–eleven translocation (TET) enzymes that use ketoglutarate as a cofactor and Fe^{2+} as an electron donor (similar to all JMJ enzymes). Hydroxymethylation of 5mhC is the obligatory step to C demethylation and transcription activation (56). Although G oxidation was the major genomic change induced by TGF-β, we notice that the global levels of 5OHmdC were higher in cells exposed for 60 and 90 min to TGF-β (Figure 3B). Collectively, G and C oxidation marks the global transcription changes induced by TGF-β during the initiation of the EMT (Figure 3).

DNA oxidation and transcription

Targeted oxidation of DNA at enhancers, TSSs and 3′ ends of genes is essential for the formation of chromatin transcription loops and the initiation complex (12,13,57). In fact, transcription loops induced by retinoic acid or estrogens do not form when LSD1 or OGG1 is downregulated or oxidation (12,13) and/or repair (12,58) are prevented. The 8-oxo-dG peak induced by 30–90-min TGF-β1 treatment corresponds to the time required to stabilize chromatin loops during initiation of transcription by estrogens or retinoic acid. These loops are RNase H sensitive, recruit LSD1, OGG1 and cohesin RAD21, and connect the enhancer–TSS and polyA sites (12,13,57). The oxidized sites form single-strand nicks that recruit topoisomerase II beta, RNA polymerase II including BER (OGG1–APE1)

and NER (12,13). These events occur in a precise temporal window (12,13,57), and histone demethylation and G oxidation are the first critical steps (12,13). We note that the punctuated oxo-dG signal detected by confocal microscopy (Figure 2A and B) resembles the interchromatin granules or nuclear speckles containing RNA splicing and transcription factors. Proteomic analysis shows that SMAD4, OGG1 and APE1 are stable components of these nuclear structures that associate transcription factories with the early RNA processing complex (59).

OGG1 was recruited to the promoter of repressed genes, including *WIF1*, at 30 and 90 min after TGF-β1 treatment. At 30 min, OGG1 was present at both the *SNAI1* and *WIF1* promoters, while at 90 min after TGF-β1 treatment OGG1 accumulated only at *WIF1* promoter (Figure 5A and B), suggesting that the second dG oxidation event, also visible by MS, was required for *WIF1* silencing. This late oxidation corresponded to the bulk of TGF-β-induced oxidation and was dependent on LSD1 (Figure 3A). Transcriptional repression by TGF-β1 was established at the *WIF1* promoter following the dissociation of the pSMAD2/3–LSD1 complex (Figure 4A). The TGF-β1 inhibitor, SB431542, prevented SMAD2/3 phosphorylation (60) and LSD1 recruitment at *SNAI1* and *WIF1* promoters (A. Pezone, unpublished data) suggesting that LSD1 targeting at TGF-β1-responsive promoters was dependent on pSMAD2/3. We suggest that LSD1 is stabilized at the *WIF1* promoter by HDAC3–NCoR1 and SNAI1 (Supplementary Figures S4B and S5B) only if there is a steady ROS signal that activates JNK. In this context, it is worth noting the following: (i) ROS activate JNK and stabilize HDAC3 bound to the *WIF1* promoter to silence the gene (38) and (ii) metabolism and ROS control JNK levels and activity (55,61). The formation of the repressor complex at the *WIF1* promoter is not trivial because it represents an important arm of the TGF-β1 signaling pathway. WIF1 is the main secreted WNT1 inhibitor and its silencing substantially amplifies WNT1 signaling and fibrosis *in vivo* (55).

Repression of EMT genes requires synchronous signaling from JNK and LSD1

LSD1 is neutral with regard to activation or repression, but it is a coincidence sensor at the *WIF1* promoter because its presence reflects a steady ROS signal leading to JNK activation and a nuclear oxidation signal, both necessary to repress transcription. In the absence of the ROS–JNK signal, LSD1 binds pSMAD2/3, activates *SNAI* transcription and marks transiently *WIF1* promoter 30 min after TGF-β1 treatment. In the presence of a persistent ROS signal (90-min TGF-β1 treatment), LSD1 binds to SNAI1–NCoR1–HDAC3 and induces a new demethylation-oxidative wave by removing activation marks from chromatin (Figure 5E). In fact, while LSD1 depletion inhibited both genes that are positively and negatively regulated by TGF-β1, transcription repression was achieved only in the presence of a concomitant and strong DPI/JNK–ROS signal. The early repressor induced by TGF-β1, SNAI1, does not repress transcription in the absence of this signal (Figure 1G and Supplementary Figure S7D). Instead, nuclear oxidation by LSD1 in the absence of JNK–ROS was sufficient to activate

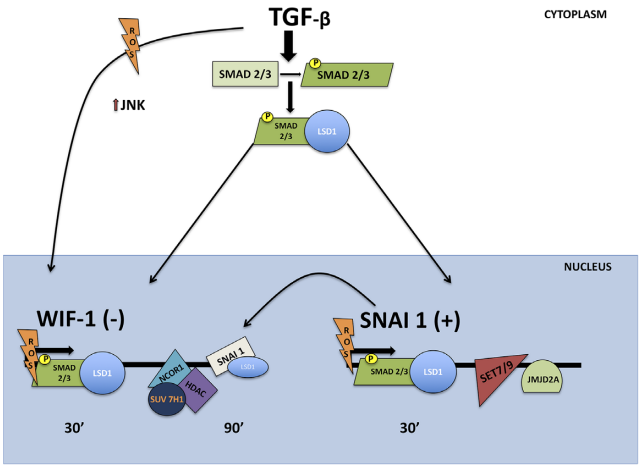

Figure 6. LSD1–phospho-SMAD2/3 complex targets genes induced or repressed by TGF-β1. Schematic cartoon summarizing the action of TGF-β1 to induce or repress transcription of EMT genes. Upon SMAD2/3 phosphorylation, induced by TGF-β1, LSD1 binds pSMAD2/3 and targets TGF-β1-inducible or -repressed genes, containing SMAD signatures (GAATCC) (37,38). Following the local DNA oxidation elicited by LSD1 and JMJD2A, 5′–3′ transcription loops and the transcription initiation complex are assembled and transcription begins (12,13,58). At the repressed genes, instead, if NOX–ROS are persistent and JNK is active, a repressor complex, containing HDAC3, NCoR1, SNAI1 and LSD1, shuts off transcription (41). At these sites, LSD1 demethylates H3k4me2 and stabilizes repression of transcription (33).

TGF-β1/EMT genes, including SNAI1 (Figure 2F and G, and Supplementary Figure S7A and C).

Initiation, establishment and maintenance of TGF-β1-induced EMT

We wish to stress that our observation window of TGF-β1 effects is narrow (0–90 min) compared to the timing of TGF-β1 action analyzed in the majority of published studies, which show that NOXs, and specifically NOX4, are essential for stable EMT (24–48 h to 15 days) (28,29). Our results complement and do not contradict the published data because the changes we document are transient and reversible. This is shown by the activation of the canonical TGF-β/SMAD pathway, which initiates a transient wave of SMAD2/3 phosphorylation (Figure 4) (60,62). In fact, if TGF-β1 is removed after 3 h to 9 days, the EMT phenotype and the induced proteins disappear. Higher doses and continuous exposure to TGF-β1 stabilize irreversibly the EMT phenotype (63); see also the comments in (64). Our data show that the early events following TGF-β1 exposure are relevant for the initiation of the EMT program and suggest that the early (1–2 h) and late (24 h) events triggered by TGF-β1 to induce EMT are mediated by a combination of different players.

We propose that the TGF-β1 EMT transcriptional program is carried out in two distinct temporal phases: the first (initiation), between 30 and 90 min, initiates the program by modifying DNA at multiple sites. On a smaller scale, the complex pSMAD2/3–LSD1 primes genomic sites that eventually will be stably activated or repressed only if the TGF-β1 signal is continuous and persistent (Figure 5) (60,63). The second phase (maintenance), between 1 and 14

days, consolidates and stabilizes TGF-β1 transcriptional repression or induction (28,29). Although we did not identify precisely the source of the DPI-sensitive ROS in the initiation phase (90-min TGF-β1 treatment), we suggest that JNK–NCoR1 and HDAC3 are essential for the stabilization and maintenance of early TGF-β1 repression of transcription (55).

Figure 6 shows a simplified scheme of the early TGF-β1 signals. It describes the induction or repression of transcription of EMT genes. Specifically, the repressor complex enucleated by LSD1 at the *WIF1* promoter inhibits transcription only when two temporally close and spatially distributed signals are present, i.e. nuclear (LSD1) and cytoplasmic (NOX–JNK) ROS. This repressor complex is an ROS sensor and is linked to the redox state of the cell (55). We speculate that the source of cytoplasmic ROS is linked to the metabolism, may vary from cell to cell and represents the so-called cell context, which substantially modifies the response to TGF-β1 in a cell-specific fashion.

SUPPLEMENTARY DATA

Supplementary Data are available at NAR Online.

ACKNOWLEDGEMENTS

This paper is dedicated to the memory of our colleagues Stelio Varrone and Rodolfo Frunzio. We thank Rita Cerillo for her help in the organization of the experiments and Max E. Gottesman for revising the manuscript.

FUNDING

Associazione Italiana per la Ricerca sul Cancro [16983, in part, to E.V.A.]; Fondazione Medicina Molecolare e Terapia Cellulare, Università Politecnica delle Marche [to E.V.A.]; Epigenomics Flagship Project—EPIGEN, CNR. Funding for open access charge: Epigenomics Flagship Project and Fondazione Cariplo.
Conflict of interest statement. None declared.

REFERENCES

1. Kalluri,R. and Weinberg,R.A. (2009) The basics of epithelial–mesenchymal transition. *J. Clin. Invest.*, **119**, 1420–1428.
2. Thiery,J.P. (2002) Epithelial–mesenchymal transitions in tumour progression. *Nat. Rev. Cancer*, **2**, 442–454.
3. Nieto,M.A. (2002) The snail superfamily of zinc-finger transcription factors. *Nat. Rev. Mol. Cell Biol.*, **3**, 155–166.
4. Cannito,S., Novo,E., Compagnone,A., Valfrè di Bonzo,L., Busletta,C., Zamara,E., Paternostro,C., Povero,D., Bandino,A., Bozzo,F. *et al.* (2008) Redox mechanisms switch on hypoxia-dependent epithelial–mesenchymal transition in cancer cells. *Carcinogenesis*, **29**, 2267–2278.
5. Taddei,M.L., Giannoni,E., Comito,G. and Chiarugi,P. (2013) Microenvironment and tumor cell plasticity: an easy way out. *Cancer Lett.*, **341**, 80–96.
6. Rhyu,D.Y., Yang,Y., Ha,H., Lee,G.T., Song,J.S., Uh,S. and Lee,H.B. (2005) Role of reactive oxygen species in TGF-beta1-induced mitogen-activated protein kinase activation and epithelial–mesenchymal transition in renal tubular epithelial cells. *J. Am. Soc. Nephrol.*, **16**, 667–675.
7. Parri,M. and Chiarugi,P. (2013) Redox molecular machines involved in tumor progression. *Antioxid. Redox Signal.*, **19**, 1828–1845.
8. Kalluri,R. and Zeisberg,M. (2006) Fibroblasts in cancer. *Nat. Rev. Cancer*, **6**, 392–401.
9. Cirri,P. and Chiarugi,P. (2011) Cancer-associated-fibroblasts and tumour cells: a diabolic liaison driving cancer progression. *Cancer Metastasis Rev.*, **31**, 195–208.
10. Giannoni,E., Bianchini,F., Masieri,L., Serni,S., Torre,E., Calorini,L. and Chiarugi,P. (2010) Reciprocal activation of prostate cancer cells and cancer-associated fibroblasts stimulates epithelial–mesenchymal transition and cancer stemness. *Cancer Res.*, **70**, 6945–6956.
11. Giannoni,E., Bianchini,F., Calorini,L. and Chiarugi,P. (2011) Cancer associated fibroblasts exploit reactive oxygen species through a proinflammatory signature leading to epithelial mesenchymal transition and stemness. *Antioxid. Redox Signal.*, **14**, 2361–2371.
12. Perillo,B., Ombra,M.N., Bertoni,A., Cuozzo,C., Sacchetti,S., Sasso,A., Chiariotti,L., Malorni,A., Abbondanza,C. and Avvedimento,E.V. (2008) DNA oxidation as triggered by H3K9me2 demethylation drives estrogen-induced gene expression. *Science*, **319**, 202–206.
13. Zuchegna,C., Aceto,F., Bertoni,A., Romano,A., Perillo,B., Laccetti,P., Gottesman,M.E., Avvedimento,E.V. and Porcellini,A. (2014) Mechanism of retinoic acid-induced transcription: histone code, DNA oxidation and formation of chromatin loops. *Nucleic Acids Res.*, **42**, 11040–11055.
14. Xiong,Y., Wang,E., Huang,Y., Guo,X., Yu,Y., Du,Q., Ding,X. and Sun,Y. (2016) Inhibition of lysine-specific demethylase-1 (LSD1/KDM1A) promotes the adipogenic differentiation of hESCs through H3K4 methylation. *Stem Cell Rev. Rep.*, **12**, 298–304.
15. Zheng,Y.C., Yu,B., Jiang,G.Z., Feng,X.J., He,P.X., Chu,X.Y., Zhao,W. and Liu,H.M. (2016) Irreversible LSD1 inhibitors: application of tranylcypromine and its derivatives in cancer treatment. *Curr. Top. Med. Chem.*, **16**, 2179–2188.
16. Hegde,V., Yadavilli,S., McLaughlin,L.D. and Deutsch,W.A. (2009) DNA repair efficiency in transgenic mice over expressing ribosomal protein S3. *Mutat. Res.*, **666**, 16–22.
17. Amente,S., Di Palo,G., Scala,G., Castrignanò,T., Gorini,F., Cocozza,S., Moresano,A., Pucci,P., Ma,B., Stepanov,I. *et al.* (2019) Genome-wide mapping of 8-oxo-7,8-dihydro-2′-deoxyguanosine reveals accumulation of oxidatively-generated damage at DNA replication origins within transcribed long genes of mammalian cells. *Nucleic Acids Res.*, **47**, 221–236.
18. Accetta,R., Damiano,S., Morano,A., Mondola,P., Paternò,R., Avvedimento,E.V. and Santillo,M. (2016) Reactive oxygen species derived from NOX3 and NOX5 drive differentiation of human oligodendrocytes. *Front. Cell. Neurosci.*, **10**, 146.
19. Gackowski,D., Starczak,M., Zarakowska,E., Modrzejewska,M., Szpila,A., Banaszkiewicz,Z. and Olinski,R. (2016) Accurate, direct, and high-throughput analyses of a broad spectrum of endogenously generated DNA base modifications with isotope-dilution two-dimensional ultraperformance liquid chromatography with tandem mass spectrometry: possible clinical implication. *Anal. Chem.*, **88**, 12128–12136.
20. Chiarugi,P., Pani,G., Giannoni,E., Taddei,L., Colavitti,R., Raugei,G., Symons,M., Borrello,S., Galeotti,T. and Ramponi,G. (2003) Reactive oxygen species as essential mediators of cell adhesion: the oxidative inhibition of a FAK tyrosine phosphatase is required for cell adhesion. *J. Cell Biol.*, **161**, 933–944.
21. Cichon,M.A. and Radisky,D.C. (2014) ROS-induced epithelial–mesenchymal transition in mammary epithelial cells is mediated by NF-κB-dependent activation of Snail. *Oncotarget*, **5**, 2827–2838.
22. Lou,Z., Wang,A.-P., Duan,X.-M., Hu,G.-H., Song,G.-L., Zuo,M.-L. and Yang,Z.-B. (2018) Upregulation of NOX2 and NOX4 mediated by TGF-β signaling pathway exacerbates cerebral ischemia/reperfusion oxidative stress injury. *Cell. Physiol. Biochem.*, **46**, 2103–2113.
23. Liu,R.-M. and Desai,L.P. (2015) Reciprocal regulation of TGF-β and reactive oxygen species: a perverse cycle for fibrosis. *Redox Biol.*, **6**, 565–577.
24. Michaeloudes,C., Sukkar,M.B., Khorasani,N.M., Bhavsar,P.K. and Chung,K.F. (2011) TGF-β regulates Nox4, MnSOD and catalase expression, and IL-6 release in airway smooth muscle cells. *Am. J. Physiol. Lung Cell. Mol. Physiol.*, **300**, L295–L304.
25. Boudreau,H.E., Casterline,B.W., Rada,B., Korzeniowska,A. and Leto,T.L. (2012) Nox4 involvement in TGF-beta and SMAD3-driven

induction of the epithelial-to-mesenchymal transition and migration of breast epithelial cells. *Free Radic. Biol. Med.*, **53**, 1489–1499.
26. Hiraga,R., Kato,M., Miyagawa,S. and Kamata,T. (2013) Nox4-derived ROS signaling contributes to TGF-β-induced epithelial–mesenchymal transition in pancreatic cancer cells. *Anticancer Res.*, **33**, 4431–4438.
27. Shanmugasundaram,K., Nayak,B.K., Friedrichs,W.E., Kaushik,D., Rodriguez,R. and Block,K. (2017) NOX4 functions as a mitochondrial energetic sensor coupling cancer metabolic reprogramming to drug resistance. *Nat. Commun.*, **8**, 997.
28. Augsburger,F., Filippova,A., Rasti,D., Seredenina,T., Lam,M., Maghzal,G., Mahiout,Z., Jansen-Dürr,P., Knaus,U.G., Doroshow,J. *et al.* (2019) Pharmacological characterization of the seven human NOX isoforms and their inhibitors. *Redox Biol.*, **26**, 101272.
29. Vincent,T., Neve,E.P.A., Johnson,J.R., Kukalev,A., Rojo,F., Albanell,J., Pietras,K., Virtanen,I., Philipson,L., Leopold,P.L. *et al.* (2009) A SNAIL1–SMAD3/4 transcriptional repressor complex promotes TGF-beta mediated epithelial–mesenchymal transition. *Nat. Cell Biol.*, **11**, 943–950.
30. Byers,L.A., Diao,L., Wang,J., Saintigny,P., Girard,L., Peyton,M., Shen,L., Fan,Y., Giri,U., Tumula,P.K. *et al.* (2013) An epithelial–mesenchymal transition gene signature predicts resistance to EGFR and PI3K inhibitors and identifies Axl as a therapeutic target for overcoming EGFR inhibitor resistance. *Clin. Cancer Res.*, **19**, 279–290.
31. Egler,R.A., Fernandes,E., Rothermund,K., Sereika,S., de Souza-Pinto,N., Jaruga,P., Dizdaroglu,M. and Prochownik,E.V. (2005) Regulation of reactive oxygen species, DNA damage, and c-Myc function by peroxiredoxin 1. *Oncogene*, **24**, 8038–8050.
32. Al-Mehdi,A.-B., Pastukh,V.M., Swiger,B.M., Reed,D.J., Patel,M.R., Bardwell,G.C., Pastukh,V.V., Alexeyev,M.F. and Gillespie,M.N. (2012) Perinuclear mitochondrial clustering creates an oxidant-rich nuclear domain required for hypoxia-induced transcription. *Sci. Signal.*, **5**, ra47.
33. Forneris,F., Binda,C., Vanoni,M.A., Mattevi,A. and Battaglioli,E. (2005) Histone demethylation catalysed by LSD1 is a flavin-dependent oxidative process. *FEBS Lett.*, **579**, 2203–2207.
34. Lin,T., Ponn,A., Hu,X., Law,B.K. and Lu,J. (2010) Requirement of the histone demethylase LSD1 in Snai1-mediated transcriptional repression during epithelial–mesenchymal transition. *Oncogene*, **29**, 4896–4904.
35. Schmidt,D.M.Z. and McCafferty,D.G. (2007) *trans*-2-Phenylcyclopropylamine is a mechanism-based inactivator of the histone demethylase LSD1. *Biochemistry*, **46**, 4408–4416.
36. Heumüller,S., Wind,S., Barbosa-Sicard,E., Schmidt,H.H.H.W., Busse,R., Schröder,K. and Brandes,R.P. (2008) Apocynin is not an inhibitor of vascular NADPH oxidases but an antioxidant. *Hypertension*, **51**, 211–217.
37. Frick,C.L., Yarka,C., Nunns,H. and Goentoro,L. (2017) Sensing relative signal in the Tgf-β/Smad pathway. *Proc. Natl Acad. Sci. U.S.A.*, **114**, E2975–E2982.
38. Zawel,L., Dai,J.L., Buckhaults,P., Zhou,S., Kinzler,K.W., Vogelstein,B. and Kern,S.E. (1998) Human Smad3 and Smad4 are sequence-specific transcription activators. *Mol. Cell*, **1**, 611–617.
39. Martin-Malpartida,P., Batet,M., Kaczmarska,Z., Freier,R., Gomes,T., Aragón,E., Zou,Y., Wang,Q., Xi,Q., Ruiz,L. *et al.* (2017) Structural basis for genome wide recognition of 5-bp GC motifs by SMAD transcription factors. *Nat. Commun.*, **8**, 2070.
40. Frederick,J.P., Liberati,N.T., Waddell,D.S., Shi,Y. and Wang,X.-F. (2004) Transforming growth factor beta-mediated transcriptional repression of c-myc is dependent on direct binding of Smad3 to a novel repressive Smad binding element. *Mol. Cell. Biol.*, **24**, 2546–2559.
41. Kang,Y., Chen,C.-R. and Massagué,J. (2003) A self-enabling TGFbeta response coupled to stress signaling: Smad engages stress response factor ATF3 for Id1 repression in epithelial cells. *Mol. Cell*, **11**, 915–926.
42. Sidorenko,V.S., Nevinsky,G.A. and Zharkov,D.O. (2007) Mechanism of interaction between human 8-oxoguanine-DNA glycosylase and AP endonuclease. *DNA Repair*, **6**, 317–328.
43. Wu,H., Min,J., Lunin,V.V., Antoshenko,T., Dombrovski,L., Zeng,H., Allali-Hassani,A., Campagna-Slater,V., Vedadi,M., Arrowsmith,C.H. *et al.* (2010) Structural biology of human H3K9 methyltransferases. *PLoS One*, **5**, e8570.
44. Dillon,S.C., Zhang,X., Trievel,R.C. and Cheng,X. (2005) The SET-domain protein superfamily: protein lysine methyltransferases. *Genome Biol.*, **6**, 227.
45. Balakrishnan,L., Brandt,P.D., Lindsey-Boltz,L.A., Sancar,A. and Bambara,R.A. (2009) Long patch base excision repair proceeds via coordinated stimulation of the multienzyme DNA repair complex. *J. Biol. Chem.*, **284**, 15158–15172.
46. Fong,Y.W., Cattoglio,C. and Tjian,R. (2013) The intertwined roles of transcription and repair proteins. *Mol. Cell*, **52**, 291–302.
47. Kozub,M.M., Carr,R.M., Lomberk,G.L. and Fernandez-Zapico,M.E. (2017) LSD1, a double-edged sword, confers dynamic chromatin regulation but commonly promotes aberrant cell growth. *F1000Research*, **6**, 2016.
48. Klose,R.J., Kallin,E.M. and Zhang,Y. (2006) JmjC-domain-containing proteins and histone demethylation. *Nat. Rev. Genet.*, **7**, 715–727.
49. Hancock,R.L., Masson,N., Dunne,K., Flashman,E. and Kawamura,A. (2017) The activity of JmjC histone lysine demethylase KDM4A is highly sensitive to oxygen concentrations. *ACS Chem. Biol.*, **12**, 1011–1019.
50. Wang,L., Chang,J., Varghese,D., Dellinger,M., Kumar,S., Best,A.M., Ruiz,J., Bruick,R., Peña-Llopis,S., Xu,J. *et al.* (2013) A small molecule modulates Jumonji histone demethylase activity and selectively inhibits cancer growth. *Nat. Commun.*, **4**, 2035.
51. Sui,A., Xu,Y., Li,Y., Hu,Q., Wang,Z., Zhang,H., Yang,J., Guo,X. and Zhao,W. (2017) The pharmacological role of histone demethylase JMJD3 inhibitor GSK-J4 on glioma cells. *Oncotarget*, **8**, 68591–68598.
52. Heinz,S., Freyberger,A., Lawrenz,B., Schladt,L., Schmuck,G. and Ellinger-Ziegelbauer,H. (2017) Mechanistic investigations of the mitochondrial complex I inhibitor rotenone in the context of pharmacological and safety evaluation. *Sci. Rep.*, **7**, 45465.
53. Wind,S., Beuerlein,K., Eucker,T., Müller,H., Scheurer,P., Armitage,M., Ho,H., Schmidt,H. and Wingler,K. (2010) Comparative pharmacology of chemically distinct NADPH oxidase inhibitors. *Br. J. Pharmacol.*, **161**, 885–898.
54. Messoussi,A., Feneyrolles,C., Bros,A., Deroide,A., Daydé-Cazals,B., Chevé,G., Van Hijfte,N., Fauvel,B., Bougrin,K. and Yasri,A. (2014) Recent progress in the design, study, and development of c-Jun N-terminal kinase inhibitors as anticancer agents. *Chem. Biol.*, **21**, 1433–1443.
55. Svegliati,S., Marrone,G., Pezone,A., Spadoni,T., Grieco,A., Moroncini,G., Grieco,D., Vinciguerra,M., Agnese,S., Jüngel,A. *et al.* (2014) Oxidative DNA damage induces the ATM-mediated transcriptional suppression of the Wnt inhibitor WIF-1 in systemic sclerosis and fibrosis. *Sci. Signal.*, **7**, ra84.
56. Rasmussen,K.D. and Helin,K. (2016) Role of TET enzymes in DNA methylation, development, and cancer. *Genes Dev.*, **30**, 733–750.
57. Pezone,A., Zuchegna,C., Tramontano,A., Romano,A., Russo,G., de Rosa,M., Vinciguerra,M., Porcellini,A., Gottesman,M.E. and Avvedimento,E.V. (2019) RNA stabilizes transcription-dependent chromatin loops induced by nuclear hormones. *Sci. Rep.*, **9**, 3925–3936.
58. Le May,N., Fradin,D., Iltis,I., Bougnères,P. and Egly,J.-M. (2012) XPG and XPF endonucleases trigger chromatin looping and DNA demethylation for accurate expression of activated genes. *Mol. Cell*, **47**, 622–632.
59. Galganski,L, Urbanek,M.O. and Krzyzosiak,W.J. (2017) Nuclear speckles: molecular organization, biological function and role in disease. *Nucleic Acids Res.*, **45**, 10350–10368.
60. Frick,C.L., Yarka,C., Nunns,H. and Goentoro,L. (2017) Sensing relative signal in the Tgf-β/Smad pathway. *Proc. Natl Acad. Sci. U.S.A.*, **114**, E2975–E2982.
61. Solinas,G. and Becattini,B. (2017) JNK at the crossroad of obesity, insulin resistance, and cell stress response. *Mol. Metab.*, **6**, 174–184.
62. Zhang,J., Tian,X.-J., Chen,Y.-J., Wang,W., Watkins,S. and Xing,J. (2018) Pathway crosstalk enables cells to interpret TGF-β duration. *npj Syst. Biol. Appl.*, **4**, 18.
63. Katsuno,Y., Meyer,D.S., Zhang,Z., Shokat,K.M., Akhurst,R.J., Miyazono,K. and Derynck,R. (2019) Chronic TGF-β exposure drives stabilized EMT, tumor stemness, and cancer drug resistance with vulnerability to bitopic mTOR inhibition. *Sci. Signal.*, **12**, eaau8544.
64. Ferrarelli,L.K. (2019) Revisiting TGF-β and EMT. *Science*, **363**, 941–943.